metals

MDPI

*Article*

# The Structural and Phase State of the TiAl System Alloyed with Rare-Earth Metals of the Controlled Composition Synthesized by the "Hydride Technology"

**Akbayan Belgibayeva [1,2,*], Yuri Abzaev [1,3], Natalia Karakchieva [1], Rakhmetulla Erkasov [2], Victor Sachkov [1] and Irina Kurzina [1]**

[1] Chemical Technology Laboratory, National Research Tomsk State University, Lenin 36, Tomsk 634050, Russia; abzaev2010@yandex.ru (Y.A.); kosovanatalia@yandex.ru (N.K.); itc@spti.tsu.ru (V.S.); kurzina99@mail.ru (I.K.)

[2] Department of Chemistry, Eurasian National University, Kazhymukan 13, Nur-Sultan 010008, Kazakhstan; erkass@mail.ru

[3] Material Research Centre for collective use, Tomsk State University of Architecture and Building, Solyanaya 2, Tomsk 634003, Russia

* Correspondence: bayan_05.06@mail.ru; Tel.: +8-775-255-8611

Received: 30 May 2020; Accepted: 22 June 2020; Published: 29 June 2020

**Abstract:** The structural state and the quantitative phase analysis of the TiAl system, alloyed with rare-earth metals synthesized using hydride technology, were studied in this work. Using the Rietveld method, the content of the major phases in the initial system Ti(50 at.%)–Al(50 at.%), as well as Ti(49 at.%)–Al(49 at.%), with alloying additions Ta, Y and Dy having a high accuracy was determined. The methods of scanning electron microscopy, transmission electron microscope and X-ray spectral microanalysis of the local areas of the structure for studying the distribution of alloying elements were used. The energies of lattices of separate phases were also determined after the full-profile specification. All the lattices of the identified structures (about 30) turned out to be stable. It was established that in the Ti(49 at.%)–Al(49 at.%) systems under study with alloying additions of metals Ta, Y and Dy, there were intermetallides composed of $AlTi_3$, TiAl in the hexagonal, tetragonal and triclinic units. It is known that after microalloying alloys by Y and Dy metals, the mass fraction of TiAl phases increases significantly (>70%).

**Keywords:** intermetallides; phase composition; microstructure; hydrides; TiAl system

## 1. Introduction

Intermetallic alloys based on γ-TiAl are a good example of the way basic and applied research along with industrial development can lead to obtaining a new innovative class of advanced structural materials [1–4]. Nowadays, intermetallic alloys based on the $\gamma$-TiAl phase are promising materials for application in aeronautical engineering, owing to their attractive properties: high specific strength, stiffness, creep resistance at temperatures of $T$ = 600–800 °C, oxidation resistance and burn resistance at temperatures up to $T$ = 900 °C. In the temperature range of $T$ = 20–800 °C, the specific modulus of elasticity of these alloys is higher than that of the nickel by 30–50% [2]. It is supposed that in the gas-turbine engine, light $\gamma$-TiAl alloys ($\rho \approx 4$ g/cm$^3$) will partially replace heat-resisting heavy nickel alloys ($\rho$ = 8–8.5 g/cm$^3$), which will allow significant increases in its specific power characteristics during a simultaneous decrease in the fuel consumption, carbon dioxide emissions and nosiness [4].

To achieve a certain combination of properties, it is necessary to optimize the chemical composition and the microstructure [4–8]. Therefore, in the past two decades, the increased focus of researchers of γ-TiAl alloys has been on achieving an optimal combination of mechanical properties by varying the elemental composition and the microstructure with various sizes of columns/grains and thickness of plates. For that, a detailed work on the optimization of the composition and conditions of thermomechanical/thermal treatment of the alloys is being performed.

In modern materials science, a new method of synthesis of binary and multicomponent alloys is of interest, which is called a "hydride" technology (HT) [9]. Modern technologies of production of alloys (mechanical alloying, arc smelting, powder metallurgy, etc.,) are associated with notable labor intensity and hardware difficulties (application of a deep vacuum and creation of inert environment at high temperatures, duration and multiplicity of processes, etc.). The powder metallurgy technique is characterized by a special duration because the result of the interaction of metals in the initial mixtures is mainly determined by solid diffusion rates. The specific difficulties of obtaining quality alloys are also associated with the presence of a dense oxide film on the surfaces of particles of refractory metals, which prevents the passage of mutual diffusion. The HT method allows the avoidance of the majority of them (in particular, it excludes melting). HT is a high-tech method based on the combination of self-propagating high-temperature synthesis SHS of transition metal hydrides and heat treatment of a mixture of hydrides, resulting in alloy formation [10–12]. In the HT method, to obtain high-strength alloys based on transition metals, the powders of hydrides of refractory metals and alloys are used as initial materials. The essence of HT consists of the successive use of processes of hydrides synthesis, their combined compacting and dehydration. The advantage of HT is that the alloy is formed at a relatively low temperature (from 900 to 1150 °C) during rapid exposition (from 1 to 2 h). It is important that metals with different values of melting temperature and density should alloy without melting [10–12]. Other advantages of the method are relative cheapness, the use of refractory materials, as well as obtaining materials with high purity. It is also known that the formation of metal alloys can be carried out easier from hydrides than from metals themselves, since chemical bonds in hydrides are less strong than bonds in metal structures [11,12].

It is well known that the compaction of the alloy structure is one of the most effective ways of improvement of strength and plasticity of the materials. Alloying was demonstrated as a viable approach to enhance the mechanical properties of TiAl alloys at room temperature through improving the materials microstructure [13,14].

To improve the mechanical properties of $\gamma$-TiAl alloys, their alloying with rare-earth elements is of interest. It is known that [15–17] the introduction of rare-earth elements (La, Er and Dy) into titanium and intermetallic alloys based on $\gamma$-TiAl can lead to the improvement in machinability in the as-cast state, owing to refinement of the structure, to increased heat-resistance and refractoriness, and in the $\gamma$-TiAl alloys, in some cases, to the enhancement of the technological plasticity at elevated temperatures.

Previous studies supposed that the addition of yttrium [18] and gadolinium [19–22] could significantly reduce the grain sizes and lamellar spaces of TiAl alloys, enhance strength and plasticity at room temperature, as well as creep resistance at high temperatures. However, the mechanisms of microstructure refinement in the rare-earth metals-modified (REM-modified) TiAl alloys were studied insufficiently because of the complex succession of solidification and solid-phase transformations of TiAl during thermal treatment and cooling [23]. Systematic data on the influence of additions of rare-earth elements on the structure and mechanical properties of $\gamma$-TiAl alloys in the literature are practically not presented.

Thus, the development of the methods for producing high-strength alloys of the TiAl system, the study of the dependence of the structural phase state on the synthesis parameters, and the study of the effect of various modifying additives on the physical and mechanical properties is an actual task.

The purpose of the present work is the development of the basics of hydride technology for the production of TiAl alloys and the study of the influence of alloying additions Ta, Y and Dy on the microstructure and the phase composition of the titanium–aluminum system obtained by the HT method. The Ti(50 at.%)–Al(50 at.%) system has been accepted as a basis of the composite material with REM additions of no more than 2 at.%.

## 2. Materials and Methods

### *2.1. Obtaining Alloys*

Samples with the following selected atomic compositions were prepared TA (TiAl); TAT (TiAlTa); TAY (TiAlY); TAD (TiAlDy). Sample TA was prepared as follows: a weighed amount of the titanium was placed in a quartz boat and heated in a furnace (Nabertherm RS 120/750/13, Lilienthal, Germany) in a stream of the hydrogen. The heating rate of the furnace was 10 °C/min to 450 °C, with a hydrogen volume flow of 500 mL/min.

This sample was cured for 3 h at this temperature; after that, it was cooled down to room temperature. The obtained metal hydrides were mixed with a nanodispersed aluminum powder (the average size of particles was 115 ± 10 nm, specific surface area—19.4 ± 3 $m^2/g$, loading of active aluminum—80.8 ± 0.6%). Then, the mixture was pressed into a round plate and was formed (collapsible compression mold, Lab Tools, diameter of 13 mm, thickness of 2 mm), pressing load was under a pressure of 5.3 tons/$sm^2$, bulk density was 3 g/$sм^3$ (Lab Tools PAH-20, 2019, St. Petersburg, Russia)). The equation for obtaining the TA sample can be written as:

$$Ti + H_2 = TiH_2 + 27.3 \text{ kcal/mole} \quad (1)$$

The TAT sample was prepared as follows: a weighed amount of the tantalum was placed in a quartz boat and heated in a furnace (Nabertherm RS 120/750/13, Lilienthal, Germany) in a stream of the hydrogen. The heating rate of the furnace was 10 °C/min to 550 °C, with a hydrogen volume flow of 500 mL/min. This sample was cured for 3 h at this temperature; after that, it was cooled down to room temperature. The equation for the production of titanium hydride can be written as:

$$2Ta + H_2 = 2TaH + 56 \text{ kcal/mole} \quad (2)$$

Titanium hydride was obtained as in the case of sample TA. Then, the obtained titanium hydride and tantalum hydride were mixed with a nanodispersed aluminum powder (according to the manufacturer, the average size of the particles was 115 ± 10 nm, specific surface area—19.4 ± 3 $m^2/g$, loading of active aluminum—80.8 ± 0.6%). Then, the mixture is pressed similar to TA.

Samples of TAY and TAD were obtained similarly to the method of obtaining TAT. The temperature for yttrium hydride and dysprosium hydride was 420 °C. The equation for obtaining a TAY sample can be written as:

$$Y + H_2 = YH_2 + 56 \text{ kcal/mole} \quad (3)$$

$$2Y + 3H_2 = 2YH_3 + 21.5 \text{ kcal/mole} \quad (4)$$

The equation for the preparation of dysprosium hydride can be written as:

$$2Dy + 3H_2 = 2DyH_3 \quad (5)$$

The obtained sample blanks were obtained in a vacuum unit and heated to a temperature of 1150 °C, with a heating rate of 2 °C/min. The vacuum value was $10^{-4}$ atm. They were maintained under these conditions for 3 h and cooled at a rate of 5 °C/min.

The equations for obtaining samples TA, TAT, TAY and TAD can be written as:

$$TiH_2 + Al = TiAl + 2H_2\uparrow \quad (6)$$

$$2TiH_2 + 2Al + 2TaH = 2TiAlTa + 3H_2\uparrow \quad (7)$$

$$TiH_2 + Al + YH_2 = TiAlY + 2H_2\uparrow \quad (8)$$

$$2TiH_2 + 2Al + 2DyH_3 = 2TiAlDy + 5H_2\uparrow \quad (9)$$

### *2.2. Research Methods*

The structural state and the quantitative phase analysis of the system TiAl-alloying metal (TA-REM), synthesized by HT, were studied in this work by the Rietveld method and scanning electron microscopy (SEM) [24,25]. Ta, Y and Dy metals were used as alloying additions. The X-ray diffraction studies of the TA-REM system were undertaken using DRON4-07 (Bourevestnik, St. Petersburg, Russia), which was modified for the digital processing of the signal. Spectra were made using copper radiation ($K_a$) according to the Bragg–Brentano scheme with an increment of 0.02°, exposure time at a point of 1 sec and in the angle range of 10–86°. The voltage on the X-ray tube was 30 kV, beam current—25 mA. The structural state and the quantitative content of the phases were identified by the Rietveld method by means of reflex [26–29]. As the standard lattices, the crystallographic data of the COD base [26] and the model structures of the TiAl system, predicted by the program code USPEX with the interface shell SIESTA [30], were used. In

connection with the promising physicochemical properties of the TiAl systems, they were alloyed with metal additions [24–34]. In this work, the search for standards of the TiAl system was supplemented by the USPEX program with the outer shell SIESTA [31,35,36].

To study the distribution of alloying elements in the structure at the local level, the quantitative X-ray spectral microanalysis of the near-surface layer, accompanied by the analysis of the microstructure and the morphology of the surface by the method of scanning electron microscopy, was carried out using the X-ray fluorescence spectral analyzer S4 Pioneer (Bruker, Karlsruhe, Germany) and the raster electron microscope "LEOEVO 50" (Zeiss, Oberkochen, Germany).

Electron microscope studies of the surface microstructure of TA-REM samples were conducted using the transmission electron microscope "JEM-2100F" (JEOL, Tokyo, Japan) with accelerating voltage of 200 kV using the attachment "JEOL" (JEOL, Tokyo, Japan), intended for energy-dispersive spectral analysis. The phases were identified applying well-known procedures using schemes of microdiffraction patterns calculated by the table values of parameters of crystalline lattices.

## 3. Results and Discussion

The USPEX-SIESTA program by means of the evolution code can predict stable structures of the known elemental composition, space group, among which the structures with the global minimum of enthalpy of the system are predicted. In the present work, the TiAl structures were used for the quantitative phase analysis. For the discovered structures (about 30) based on complete structural information, the energies of lattices were calculated proceeding from the first principles. All the lattices turned out to be stable and they were used at the next stage for qualitative and quantitative phase analysis by the Rietveld method. In Tables 1–5, there are standards in the initial state, obtained from the COD base ($AlTi_3$, AlTi), as well as the structure predicted by means of the USPEX code (TiAl-Struct2, AlTi3-2768). For the alloy with the conventional designation TiAl-Struct2, AlTi3-2768, the energy was calculated in the framework of the electron density functional by the gradient pseudo potential of electron density (GGA). The details of the code are given in the work of reference [26]. The total energy of the lattices was determined at 0 K. Wave functions of valence electrons of TiAl-Struct2 atoms were analyzed on the basis of flat waves with a cutoff radius of kinetic energy of 330 eV. In this case, the convergence of the total energy was ~ $0.5 \times 10^{-6}$ eV/atom. It was established that the lattice energy after geometric optimization turned out to be equal to $E_{TiAl\text{-}Struct11} = -4978.555$ eV, and in the initial state −4976.099 eV. The final enthalpy of the TiAl-Struct2 structure in both cases is evidence of its stability. TiAl lattices ($AlTi_3$-2768) with Y, Ta and Dy additives (Tables 2–4) also turn out to be stable, and the lattice energies are substantially negative. In this work, based on the results of the qualitative phase analysis of the TA-REM system, it was suggested that the REM nanoadditions were embedded into the interstitial site [0.5 0.5 0.5] of the lattice of the $AlTi_3$ alloy. Quantum chemical calculations of the $AlTi_3$ energy in the initial state, as well as with the embedded nanoadditions in the mentioned site, were made. It was established that: $E_{AlTi3} = -19{,}318.285$ eV; $E_{AlTi3\text{-}Y} = -19{,}712.792$ eV; $E_{AlTi3\text{-}Ta} = -19{,}613.620$ eV; $E_{AlTi3\text{-}Dy} = -31{,}227.561$ eV.

The calculations are evidence of the fact that the introduction of the alloying metals into the indicated interstitial site is possible and it leads to the significant stabilizing effect of the lattices in each TA-REM system without exception. In fact, the binding energy of ($|E_{AlTi3}|$) atoms in the lattices accompanied by the addition of the alloying metal increased significantly. It is interesting to note that the increase in the binding energy is accompanied by significant polarization of the Millikan charges [37,38]. The Millikan charges in the metal additions are equal: [(−5.96)Y], [(−4.42)Ta], [(+0.73)Dy], but on the atoms of the main elements—[(−0.16)Al, (+1.540)Ti], [(−0.35)Al, (+1.22)Ti], [(−0.13)Al, (−0.12)Ti], [(−0.17)Al, (−0.13)Ti] in ternary compounds TAT, TAY and TAD, respectively. The analysis of distances between atoms of the main elements and additions showed that these distances were significantly less than the sum of the covalent radii of free elements Ti and Al, and Ta, Y and Dy, which are equal, respectively, to 1.6, 1.21, 1.7, 1.90, 1.92Å [39]. For instance, in the TAT system, the lengths of bonds TiTa and AlTa are equal to 2.030 and 2.031 Å, respectively. Polarization of the charges is indicative of the growth in the share of the covalent bond as a result of introduction of the alloying metals.

The results of the quantitative content of phases in the studied systems are given in Tables 1–4. The tables show the phases, the structural state of the phases before (Init) and after (Spec) the Rietveld refinement of the experimental diffractograms, the corresponding lattice parameters, the lattice volume

(V), the space group, the fraction of the individual phases (Share) and the lattice energy after refinement by the Rietveld method (E). The tables also show the fraction of the calculated integrated intensity (Rwp) in the experimental diffractogram. The analysis of the contributions into the integral intensity of separate phases (Table 1, Figure 1) showed that to a high degree of reliability ($R_{wp}$ < 7.2%), the major phases were intermetallides $AlTi_3$, $AlTi_3$-REM, AlTi and TA-Struct2 in the initial and optimized states. The experimental diffraction patterns of the TA, TAT, TAY and TAD systems can be approximated well by the calculated integral intensity; the difference between them is an insignificant value (Figure 1). However, as Tables 1–4 show, the contributions of separate phases differ in different systems. Using the Rietveld method, it is established that in the TA system, the contribution of the triclinic TiAl system (over 73%) predominates. Both lattices differ by parameters, atoms coordinates, as well as the volume (Table 1). The number of the main systems also includes the hexagonal lattice of $AlTi_3$ (22.33%). The introduction of an insignificant amount of Ta, Y and Dy leads to the redistribution of the contributions of the hexagonal and triclinic systems. In the TA-REM systems, the contribution of the geometrically optimized lattice (TA-Struct2-GeomOpt) disappears, and the phase with the AlTi tetragonal lattice appears (Tables 2–4). The introduction of Ta into the $AlTi_3$ lattice significantly increases its binding energy and stimulates the contribution to the integral intensity up to 26.99%. On the contrary, in the TAY and TAD systems, additions Y and Dy lead to the reduction in the share of $AlTi_3$ to 16.66, 4.78 and 11.20%, respectively. The share of phases and the energy of the lattices allow evaluation of the effective energy of the TA, TAT, TAY and TAD systems according to the formula $\alpha E_1+\beta E_2+\gamma E_3$, where $\alpha$, $\beta$, $\gamma$—the share of phases; $E_1$, $E_2$, $E_3$—the energy of the lattices of separate phases. It was established that the energies of the mentioned systems were equal to −7907.453, −5407.31, −7341.104, −21,188.219 and −15,920.023 eV, respectively.

The relative coordinates of the atoms and isotropic parameters of displacements are given in Tables(5-6). The lattice parameters and space group are shown in Tables (1–4).

**Table 1.** Structural parameters of the lattices and the share of phases, and the convergence criterion of the TA alloy.

| Phase | State | a, Å | b, Å | c, Å | alpha | beta | gamma | V, A^3 | Space group | Share, % | E, eV | Rwp, % |
|---|---|---|---|---|---|---|---|---|---|---|---|---|
| $AlTi_3$-2768 | Init. | 5.764 | 5.764 | 4.664 | 90.00 | 90.00 | 120.00 | 132.56 | P6/mmm, Hexagonal | 22.33 | −19,317.484 | 7.193 |
| | Spec. | 5.763 | 5.763 | 4.645 | 90.00 | 90.00 | 120.00 | 131.996 | | | | |
| TiAl-Struct2-GeomOpt | Init. | 6.339 | 4.150 | 4.234 | 113.36 | 93.36 | 92.52 | 132.56 | P1, Triclinic | 49.80 | −4810.6263 | |
| | Spec. | 6.129 | 4.237 | 4.017 | 113.62 | 88.24 | 92.42 | 133.711 | | | | |
| TiAl-Struct2 | Init. | 6.339 | 4.150 | 4.234 | 113.36 | 93.36 | 92.52 | 101.791 | P1, Triclinic | 24.08 | −4975.776 | |
| | Spec. | 6.194 | 4.119 | 4.215 | 113.07 | 92.88 | 91.97 | 98.64 | | | | |

**Table 2.** Structural parameters of the lattices and the share of phases, and the convergence criterion of the TAY alloy.

| Phase | State | a, Å | b, Å | c, Å | alpha | beta | gamma | V, A^3 | Space group | Share % | E, eV | Rwp, % |
|---|---|---|---|---|---|---|---|---|---|---|---|---|
| $AlTi_3$-2768 | Init. | 5.764 | 5.764 | 4.664 | 90.00 | 90.00 | 120.00 | 132.56 | P6/mmm, Hexagonal | 26.99 | −19,603.151 | 6.317 |
| | Spec. | 5.736 | 5.736 | 4.626 | 90.00 | 90.00 | 120.00 | 131.828 | | | | |
| AlTi-2770 | Init. | 2.837 | 2.837 | 4.059 | 90.00 | 90.00 | 90.00 | 32.677 | P4/mmm, Tetragonal | 41.04 | −1660.340 | |
| | Spec. | 2.824 | 2.824 | 4.070 | 90.00 | 90.00 | 90.00 | 32.466 | | | | |
| TiAl-Struct2 | Init. | 6.339 | 4.150 | 4.234 | 113.36 | 93.36 | 92.52 | 101.791 | P1, Triclinic | 27.63 | −4954.073 | |

| | | | | | | | | |
|---|---|---|---|---|---|---|---|---|
| | Spec. | 6.245 | 4.128 | 4.319 | 114.67 | 91.27 | 93.84 | 100.802 |

**Table 3.** Structural parameters of the lattices and the share of phases, and the convergence criterion of the TAT alloy.

| Phase | State | a, Å | b, Å | c, Å | alpha | beta | gamma | V, A^3 | Space group | Share, % | E, eV | Rwp, % |
|---|---|---|---|---|---|---|---|---|---|---|---|---|
| $AlTi_3$-2768 | Init. | 5.764 | 5.764 | 4.664 | 90.00 | 90.00 | 120.00 | 132.56 | P6/mmm, Hexagonal | 16.66 | −19,705.872 | 6.701 |
| | Spec. | 5.791 | 5.791 | 4.736 | 90.00 | 90.00 | 120.00 | 137.565 | | | | |
| AlTi-2770 | Init. | 2.837 | 2.837 | 4.059 | 90.00 | 90.00 | 90.00 | 32.677 | P4/mmm, Tetragonal | 50.61 | −1660.341 | |
| | Spec. | 2.831 | 2.831 | 4.067 | 90.00 | 90.00 | 90.00 | 32.609 | | | | |
| TiAl-Struct2 | Init. | 6.339 | 4.150 | 4.234 | 113.36 | 93.36 | 92.52 | 101.791 | P1, Triclinic | 25.79 | −4978.726 | |
| | Spec. | 6.568 | 4.133 | 4.093 | 160.27 | 95.85 | 92.64 | 33.821 | | | | |

**Table 4.** Structural parameters of the lattices and the share of phases, and the convergence criterion of the TAD alloy.

| Phase | State | a, Å | b, Å | c, Å | alpha | beta | Gamma | V, A^3 | Space group | Share, % | E, eV | Rwp, % |
|---|---|---|---|---|---|---|---|---|---|---|---|---|
| $AlTi_3$-2768 | Init. | 5.764 | 5.764 | 4.664 | 90.00 | 90.00 | 120.00 | 132.56 | P6/mmm, Hexagonal | 11.20 | −31,228.526 | 6.504 |
| | Spec. | 5.771 | 5.771 | 4.657 | 90.00 | 90.00 | 120.00 | 134.34 | | | | |
| AlTi-2770 | Init. | 2.837 | 2.837 | 4.059 | 90.00 | 90.00 | 90.00 | 32.677 | P4/mmm, Tetragonal | 65.04 | −1660.341 | |
| | Spec. | 2.826 | 2.826 | 4.074 | 90.00 | 90.00 | 90.00 | 32.537 | | | | |
| TiAl-Struct2-GeomOpt | Init. | 6.339 | 4.145 | 4.234 | 113.36 | 93.36 | 92.52 | 101.79 | P1, Triclinic | 16.88 | −4978.606 | |
| | Spec. | 6.294 | 4.139 | 4.260 | 115.23 | 92.72 | 91.94 | 100.09 | | | | |

**Table 5.** Relative coordinates of the atoms in the TiAl-Struct2 lattice.

| Symbol of the atom | x | y | z | Displacement parameters, (U_iso) | Occupancy |
|---|---|---|---|---|---|
| Ti1 | 0.310 | −0.359 | −0.678 | 0.0127 | 1.0 |
| Ti2 | −0.500 | 0.334 | 0.667 | 0.0127 | 1.0 |
| Ti3 | −0.311 | 0.027 | 0.012 | 0.0127 | 1.0 |
| Ti4 | 0.227 | −0.017 | −0.036 | 0.0127 | 1.0 |
| Al5 | −0.000 | 0.334 | −0.333 | 0.0127 | 1.0 |
| Al6 | −0.227 | −0.316 | 0.370 | 0.0127 | 1.0 |

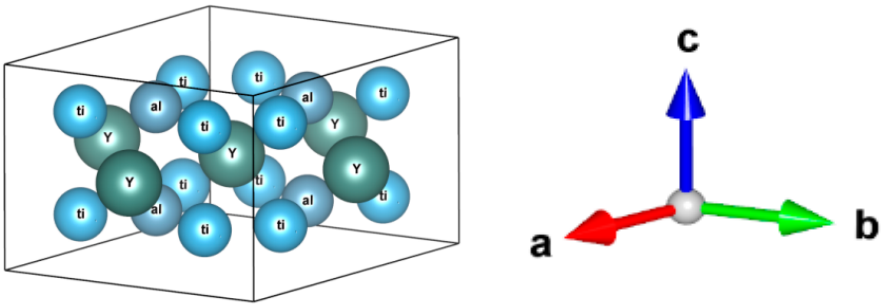


**Figure 1.** 3D lattice of the $AlTi_3$ alloy with the Y atom embedded in the site [0.5 0.5 0.5].

**Table 6.** Relative atomic coordinates in the AlTi lattice ($AlTi_3$-2768) with an embedded atom Dy, Ta and Y.

| Element | x | y | z | U_iso | occupancy |
|---|---|---|---|---|---|
| Ti | 0.833 | 0.167 | 0.25 | 0.0127 | 1 |
| Al | 0.333 | 0.667 | 0.25 | 0.0127 | 1 |
| Dy; Ta; Y | 0.5 | 0.5 | 0.5 | 0.0127 | 1 |

Figure 2 shows the results of the observed and calculated intensities of the initial alloy and alloys obtained by doping with rare-earth metals. X-ray phase analysis of the samples obtained by doping with rare-earth metals showed that they have a complex multiphase structure: the initial components (Ti, Al) and the new phases—intermetallic phases $AlTi_3$, $AlTi_3$–REM, AlTi, TiAl-Struct2—in the initial and optimized states were identified.

The study of the microstructure showed that the base of the material was the alloy of titanium and aluminum with a small quantity of alloying metals (no more than 2 at.%). The ratio between the atomic concentrations of Al and Ti is close to the initial 1:1 (Figures 3). The spectra of characteristic X-ray radiation are also given in Figure 3.

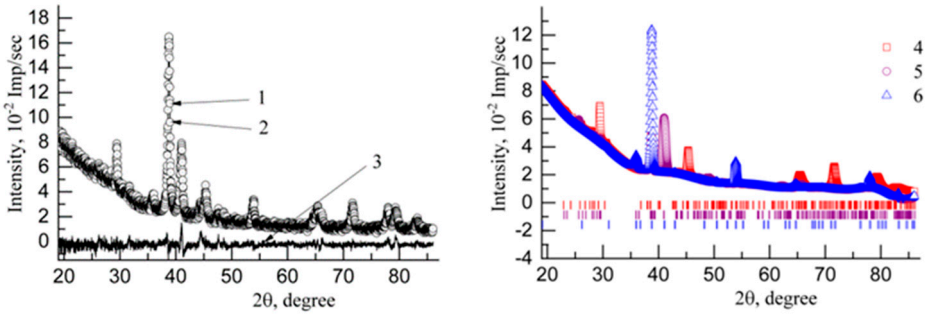


(**a**) TA (**b**) TA

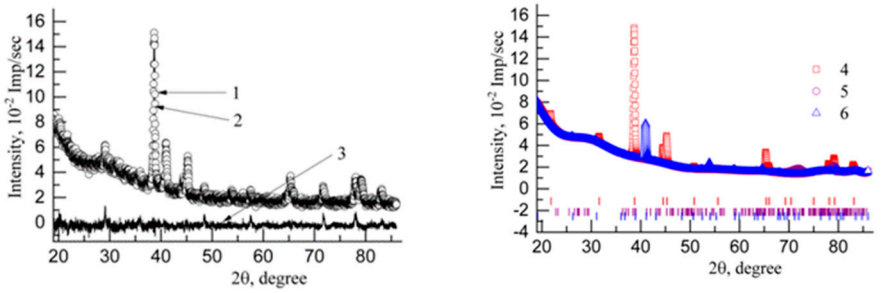


(**c**) TAY (**d**) TAY

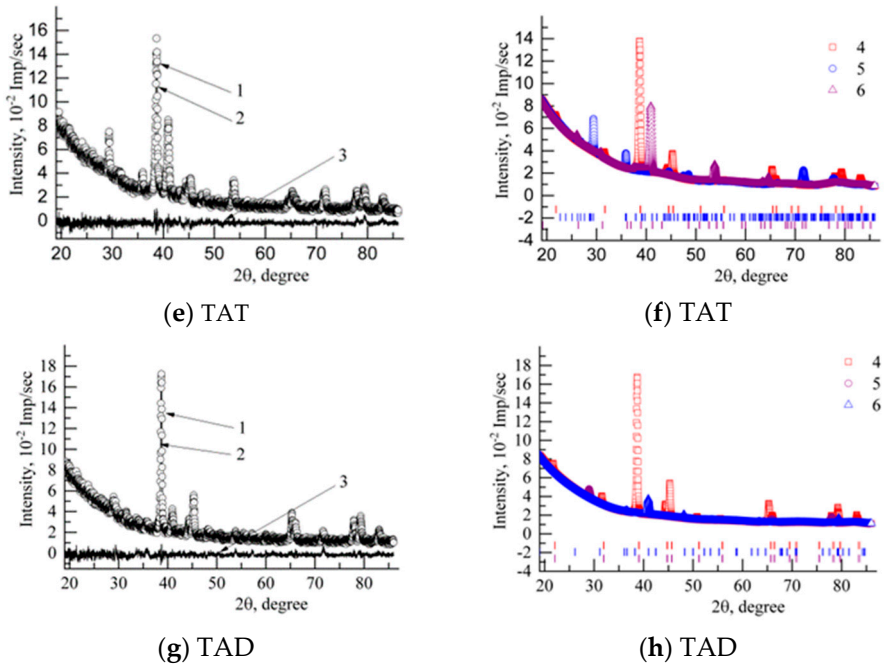


(**e**) TAT (**f**) TAT

(**g**) TAD (**h**) TAD

**Figure 2.** Diffraction patterns of alloys TA(**a**,**b**); TAY (**c**,**d**); TAT (**e**,**f**); TAD (**g**,**h**): 1—experiment, 2—summary model intensity, 3—difference between intensities, 4–6—contributions to the integral intensity of separate phases.

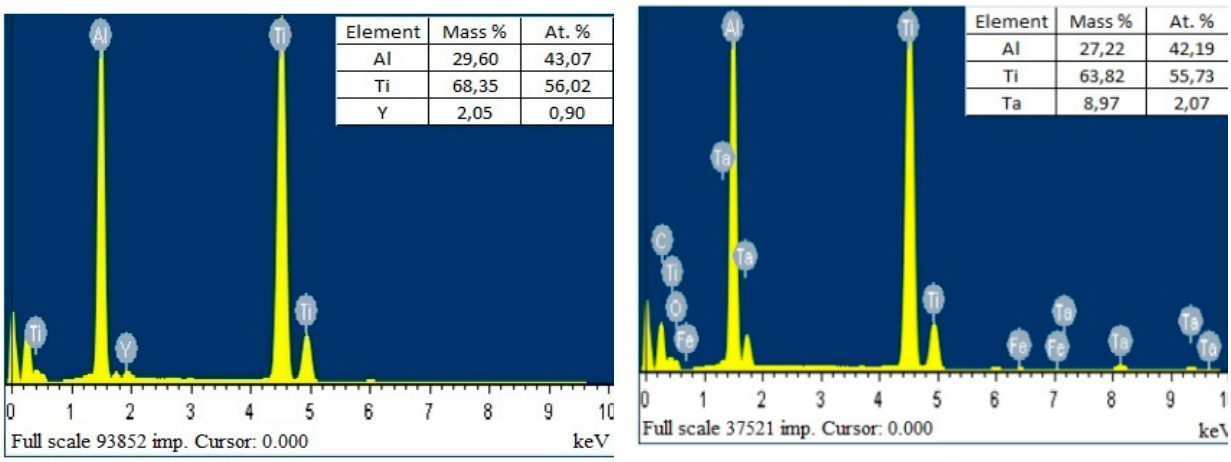


(**a**) (**b**)

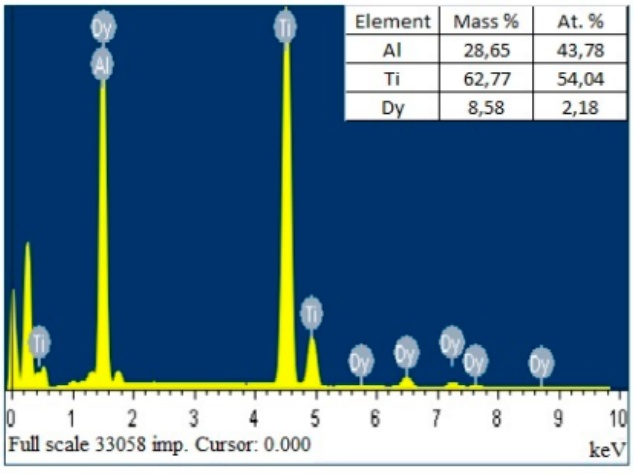


(**c**)

**Figure 3.** EDX-spectra and elemental composition of the TAY (**a**), TAT (**b**) and TAD (**c**) alloys.

As a result of the quantitative analysis, it was established that the matrix of the TAY alloy on average had a composition in mass percent: 29.60% of Al and 68.35% of Ti, which corresponds to the intermetallide phase $\alpha_2$-$Ti_3Al$ according to the stoichiometric ratio (Figure 3a). The elemental analysis of the TAT and TAD alloys (Figure 3b,c) also revealed the presence of titanium aluminide $\alpha_2$-$Ti_3Al$. This agrees with the results obtained in the works [40,41]. It was established that the microstructure of the rest of the alloys was also characterized by the formation of the $\alpha_2$-$Ti_3Al$ intermetallide.

The choice of these metals as alloying microadditions in the alloys under study is conditioned by a number of positive effects. In particular, metals as an effective modifier of the cast structure [15–22] possess an increased affinity with oxygen, which in turn leads to a substantial decrease in the amount of oxygen in the alloy and, as a consequence, to an increase in low-temperature plasticity because of the reduction in the number of barriers in the form of oxygen atoms, which decelerate the dislocations motion during deformation.

The X-ray phase analysis results of the initial intermetallic alloy TA showed that the basic thermodynamically stable phases were intermetallide compounds $Ti_3Al$, TiAl, $TiAl_2$ and a solid aluminum solution in titanium $\alpha$-Ti (Table 7).

**Table 7.** Crystallographic data of phases in the system TA.

| Composition | Space group | Syngony | CSR volume, Å^3 | Weight fraction, % | Lattice parameters, Å | | |
|---|---|---|---|---|---|---|---|
| | | | | | a | b | c |
| TiAl | *P4/mmm* | tetragonal | 33 ± 5 | 38.4 | 2.8234 | 2.8234 | 4.0768 |
| $Ti_3Al$ | P63/mmc | tetragonal | 134 ± 5 | 25.2 | 5.7671 | 5.7671 | 4.64646 |
| $\alpha$-Ti | *C6/mmc* | hexagonal | 31 ± 5 | 18.0 | 2.9253 | 2.9253 | 4.6184 |
| $TiAl_2$ | *C/mmm* | rhombic | 195 ± 5 | 11.8 | 12.0187 | 4.0232 | 4.0253 |
| $Ti_5Al_{11}$ | *P/mmm* | rhombic | 261 ± 5 | 8.3 | 3.9522 | 3.9522 | 17.3119 |
| $Ti_3Al_5$ | *P/mmm* | rhombic | 61 ± 5 | 2.9 | 3.8675 | 3.8212 | 4.1445 |
| $Ti_2Al_5$ | P4/mmm | tetragonal | 440 ± 5 | 2.5 | 3.8164 | 3.8164 | 30.1785 |

A small fraction of the sample consists of the following intermediate phases having practically constant chemical compositions: $Ti_5Al_{11}$, $Ti_3Al_5$, $TiAl_2$, $Ti_2Al_5$. The X-ray phase analysis (XPA) results are confirmed by TEM studies. The TEM studies showed that, before the introduction of rare-earth metals, in the initial state, the TA alloy contained phases $Ti_3Al$, TiAl, $TiAl_2$, $\alpha$-Ti, $Ti_5Al_{11}$ and $Ti_3Al_5$ (Figure 4e). Consequently, the obtained TA alloy has a complex multiphase structure, as it contains a number of phases with different crystal lattices. This fact confirms a possibility of obtaining intermetallic alloys by hydride technology.

First of all, the obtained studies of the microstructure confirmed the formation of $Ti_3Al$ and TiAl phases. The $Ti_3Al$ phase is an ordered phase with a D019 superstructure having an HCP crystal lattice; its space group is *P63/mmc*. $Ti_3Al$ is formed as parallel lamellar precipitates (Figure 4a). The intermetallide $Ti_3Al$ and TiAl phases under formation are microdimensional, which is evident owing to the dark-field images (Figure 4c,d). The presence of $Ti_3Al$ and TiAl is associated with thermodynamics of the phases' formations. The formation of these phases is characterized by a minimum of Gibbs energy [42]. The existence of these intermetallide phases must result in significant alloy strengthening [6,43,44].

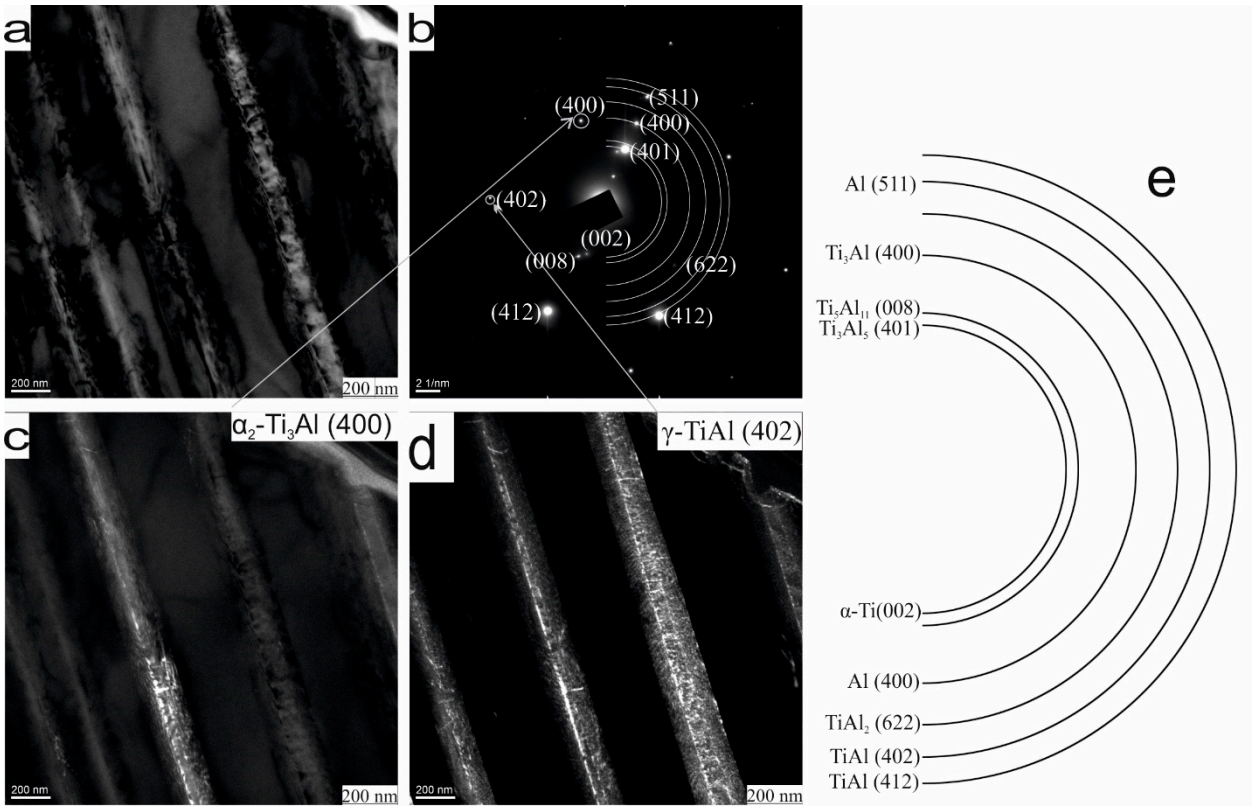


**Figure 4.** Electron microscope images of the matrix of the initial alloy TA: (**a**) bright-field image; (**b**) microdiffraction pattern; (**c**), (**d**) dark-field images in reflexes, marked by arrows; (**e**) microdiffraction pattern identification.

A layer-by-layer location of intermetallide phases—that is, alternation by the composition—is possible. Thus, using hydride technology allows for obtaining of complex sandwich structures. Owing to alternation of intermetallide phases, it becomes possible to obtain super strong materials, where each layer strengthens the previous one.

To predict the composition of the formed phases when microalloying the TiAl alloys with rare-earth metals, ternary diagrams of the corresponding ternary systems were considered. The analysis of the TiAlY ternary diagram of the partial isothermal cross-section at 1000 °C shows that the content of the Ti:Al:Y = 49:49:2 components corresponds to the highlighted area of formation of γ-TiAl + $YAl_2$ phases (Figure 5). The ternary diagram of the TiAlTa system at 1100 °C implies that at a ratio of Ti:Al:Ta = 49:49:2 components the TiAl phase is formed (Figure 5c). According to the ternary diagram, TiAlDy at a ratio of components Ti:Al:Dy = 49:49:2, the formation of the area, where $DyAl_2$ + TiAl phases are present, can be expected (Figure 5b).

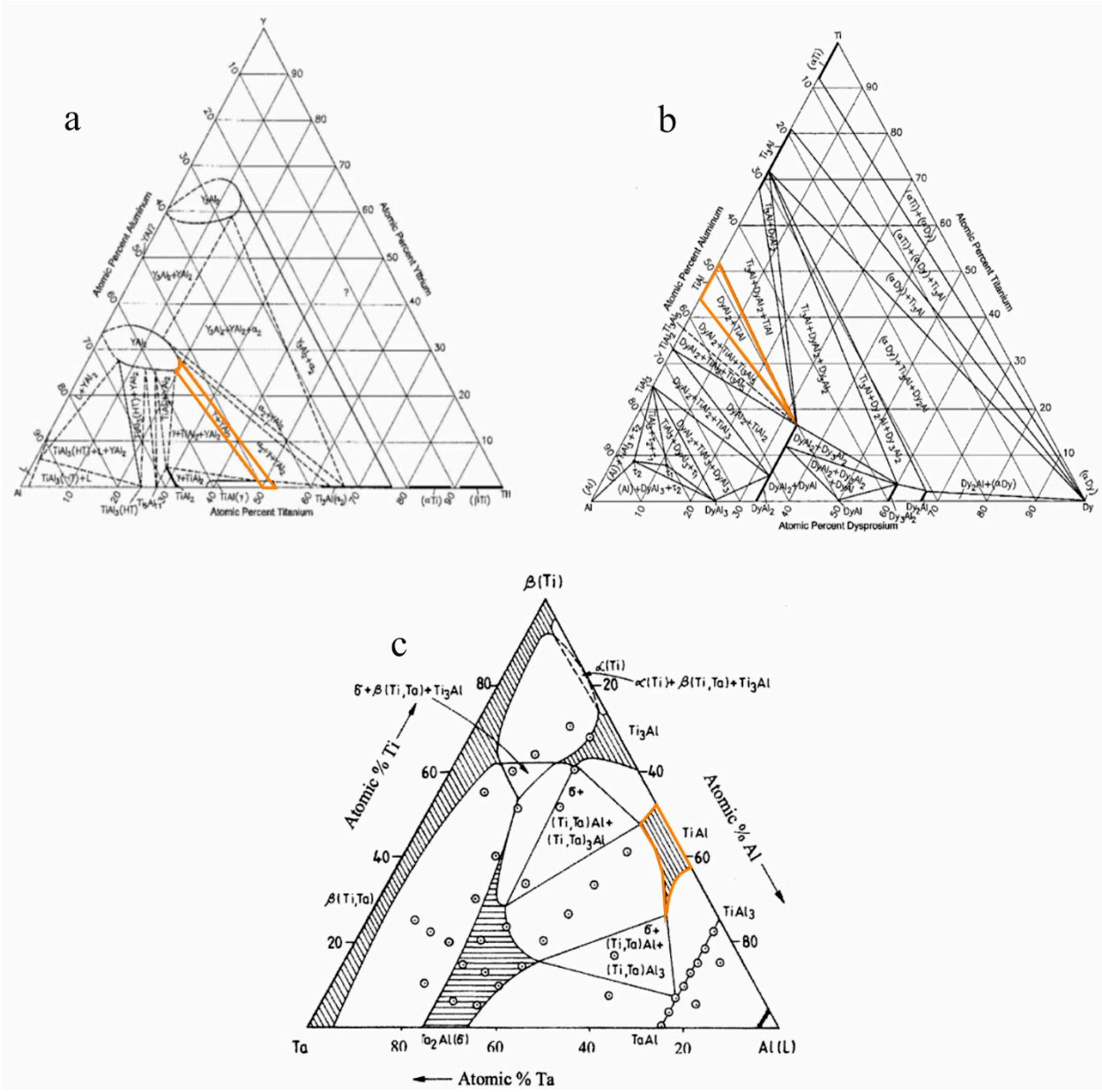


**Figure 5.** Isothermal cross-sections of the TiAlY system at 1000 °C [45] (**a**), of the TiAlDy system at 500 °C [46] (**b**), of the TiAlTa system at 1100 °C [47] (**c**).

The X-ray phase analysis of the samples, obtained during alloying with yttrium, is given in Table 8.

**Table 8.** Crystallographic data of phases in the TAY system.

| Composition | Space group | Syngony | CSR volume, Å^3 | Weight fraction, % | Lattice parameters, Å | | |
|---|---|---|---|---|---|---|---|
| | | | | | a | b | c |
| $Ti_3Al_5$ | *P/mmm* | rhombic | 65 ± 5 | 70.3 | 4.0040 | 4.0049 | 4.0710 |
| $Ti_3Al$ | P63/mmc | tetragonal | 134 ± 5 | 18.3 | 5.7661 | 5.7661 | 4.6371 |
| Al | Fm-3m | cubic | 66±5 | 8.6 | 4.0311 | 4.0311 | 4.0311 |
| α-Ti | *P63/mmc* | hexagonal | 31 ± 5 | 1.4 | 2.9186 | 2.9186 | 4.6006 |
| TiAl | *P4/mmm* | tetragonal | 40 ± 5 | 1.2 | 2.7453 | 2.7453 | 5.3402 |
| Y | P63/mmc | hexagonal | 67± 5 | 0.3 | 3.6689 | 3.6689 | 5.7302 |

According to the XPA data, the TAY alloy contains the basic $Ti_3Al_5$ phase. The $Ti_3Al_5$ phase has a rhombic crystal lattice and the space group P/mmm. Along with the $Ti_3Al_5$ grains, the structure of the alloy

contains a small number of grains of the $Ti_3Al$ phase, having an HCP crystal lattice and the space group P63/mmc. A small fraction belongs to phases TiAl, Al, $\alpha$-Ti and Y.

Figure 6 presents electron microscope images of the TAY alloy. On the microdiffraction pattern (Figure 6b), there are reflexes belonging to planes (110) and (201) TiAl; (101), (200), (302), (411) $Ti_3Al$; (400) $Ti_3Al_5$; (311) $YAl_2$; (100) $\alpha$–Ti; (200) Al. Thus, the XPA results are confirmed by TEM.

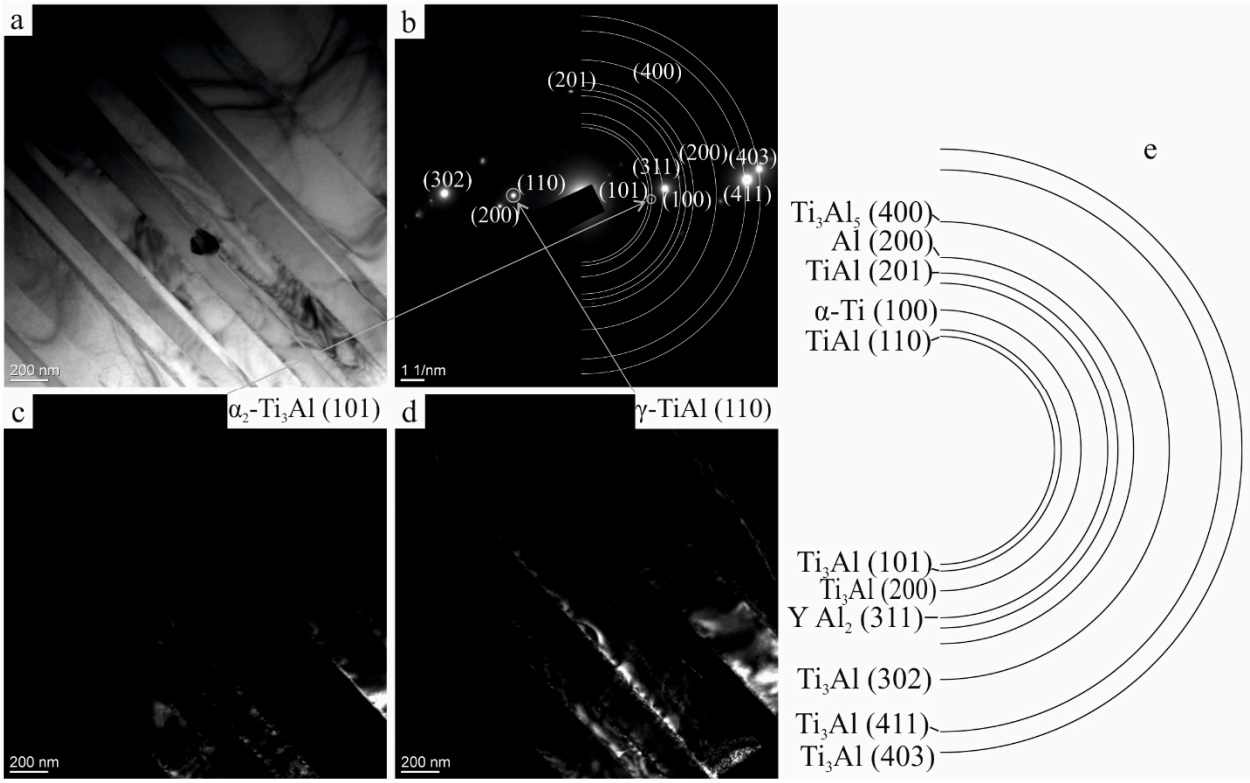


**Figure 6.** Electron microscope images of the TAY alloy: (**a)** bright-field image; (**b)** microdiffraction pattern; (**c**,**d**) dark-field images in reflexes, marked by arrows; (**e)** microdiffraction pattern identification.

Figure 7 presents TEM images of the depositions of yttrium particles of different shapes inside the grain of titanium aluminide. According to the TEM results, yttrium and Al form the $YAl_2$ intermetallide in intermetallide phases and are located on dislocations or on grain boundaries.

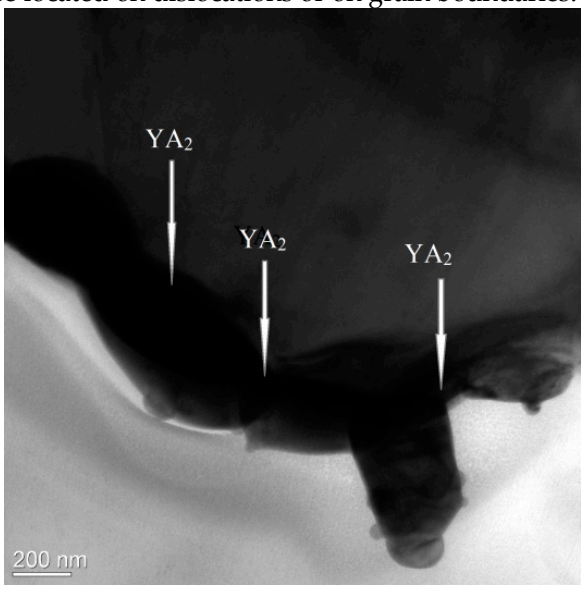


**Figure 7.** TAY alloy microstructure.

The X-ray phase analysis of the samples obtained when alloying with dysprosium (TAD) and tantalum (TAT) showed that these alloys had a complex multiphase structure: initial components Al, $\alpha$-Ti and new phases—intermetallide phases TiAl, $Ti_3Al$, $Ti_5Al_{11}$, Ti3Al5—were identified (Table 9). The basic phase of the TAD alloy is the TiAl phase, which has an ordered tetragonal-distorted face-centered structure and the P4/mmm space group.

The results of the X-ray phase analysis of the TAT alloy showed that in the alloy, the main share belonged to intermetallide phases: 30.1% of titanium aluminide TiAl of tetragonal syngony with the space group P4/mmm; 22.9% of the $Ti_3Al$ phase, having a space-centered lattice of tetragonal syngony with the space group P63/mmc; 26.4% of the $Ti_3Al_5$ phase with the space group P/mmm (Table 9). The smallest share belongs to 1.9% of $Ti_2Al_5$ with the space group P4/mmm and 3.9% of $Ti_5Al_{11}$ with the space group P/mmm. In addition, the intermetallide of tantalum and aluminum ($Ta161_{,8}Al_{282,2}$) is present in the sample.

**Table 9.** Crystallographic data of phases in the TAD and TAT systems.

| Alloy | Composition | Space group | Syngony | Weight fraction, % | Alloy | Composition | Space group | Syngony | Weight fraction, % |
|---|---|---|---|---|---|---|---|---|---|
| TAD | TiAl | *P4/mmm* | tetragonal | 74.3 | TAT | TiAl | *P4/mmm* | tetragonal | 30.1 |
| | $Ti_3Al_5$ | *P/mmm* | rhombic | 10.9 | | $Ti_3Al$ | P63/mmc | tetragonal | 22.9 |
| | $TiAl_2$ | *C/mmm* | rhombic | 5.0 | | $Ti_3Al_5$ | *P/mmm* | rhombic | 26.4 |
| | Al | Fm-3m | cubic | 3.9 | | $Ti_5Al_{11}$ | *P/mmm* | rhombic | 3.9 |
| | $Ti_5Al_{11}$ | *I4/mmm* | rhombic | 1.4 | | $\alpha$-Ti | *P63/mmc* | hexagonal | 3.9 |
| | $\alpha$-Ti | *P63/mmc* | hexagonal | 1.4 | | $TaAl_3$ | F-43m | cubic | 2.8 |
| | Dy | *P63/mmc* | hexagonal | 1,6 | | $Ti_2Al_5$ | P4/mmm | tetragonal | 1.9 |

The results of the X-ray phase analysis of the TiAlDy alloy are confirmed by the TEM results (Figure 8). On the microdiffraction pattern there are reflexes belonging to planes (002), (004), (402), (413) TiAl; (600), (203) and (423) $Ti_3Al$; (312) $TiAl_2$; (008) $Ti_5Al_{11}$; (511) Al; (300) $\alpha$-Ti; (551) $DyAl_2$.

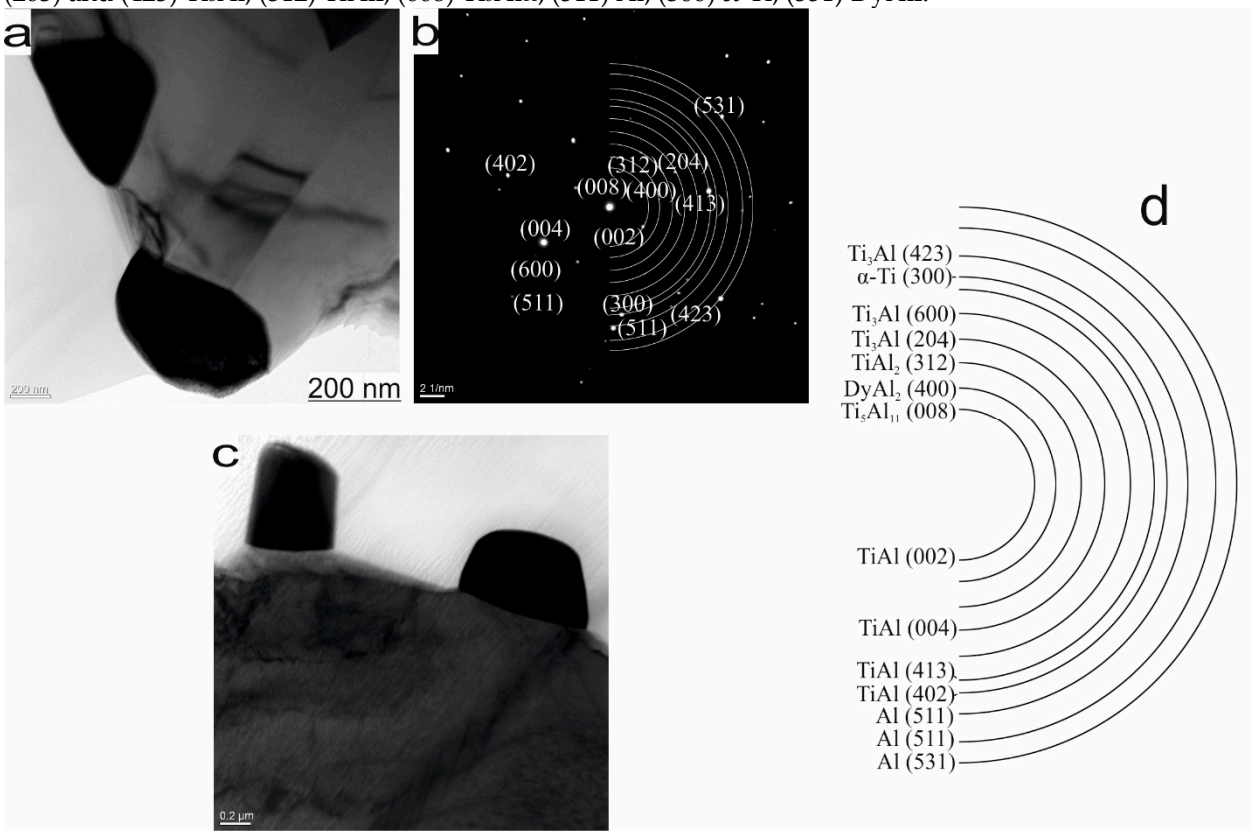


**Figure 8.** Electron microscope images of the TAD alloy: (**a)** bright-field image; (**b)** microdiffraction pattern; (**c)** dark-field images in the reflex; (**d)** microdiffraction pattern identification.

Figure 9 shows the electron microscope images of the TAT alloy. According to the microdiffraction analysis in the layers of the TAT alloy, there are the following intermetallide phases with reflexes belonging to planes (312), (412) TiA; (110), (402) and (210) $Ti_3Al$; (311), (440) $Ti_3Al_5$; (314) $Ti_5Al_{11}$; (103) $\alpha$-Ti; (008) and (215) $TaAl_3$.

Thus, the TEM studies confirmed the formation of a number of phases of titanium aluminide. The tantalum compounds indicated by the XPA method probably remain in the volume of the sample, but only $TaAl_3$ is present in the film structure.

As Ti and Ta have significant solubility in Al, Ta can form a solid substitutional solution in titanium and contribute to formation of the Widmanstatten microstructure. In addition, it is well known that the TaAl system also dissolves Ti (Ti aluminide) by as much as 60 at.%. Aluminides TiAl and $Ti_3Al$ dissolve Ta (Ta aluminide) up to 10 and 15 at.%, respectively [47–49]. The TEM research results comply with the data of the X-ray phase analysis, which imply that an insignificant amount of Ta dissolves in the crystals of TiAl and $Ti_3Al$ and are present in the $(Ti,Ta)Al_3$ phase.

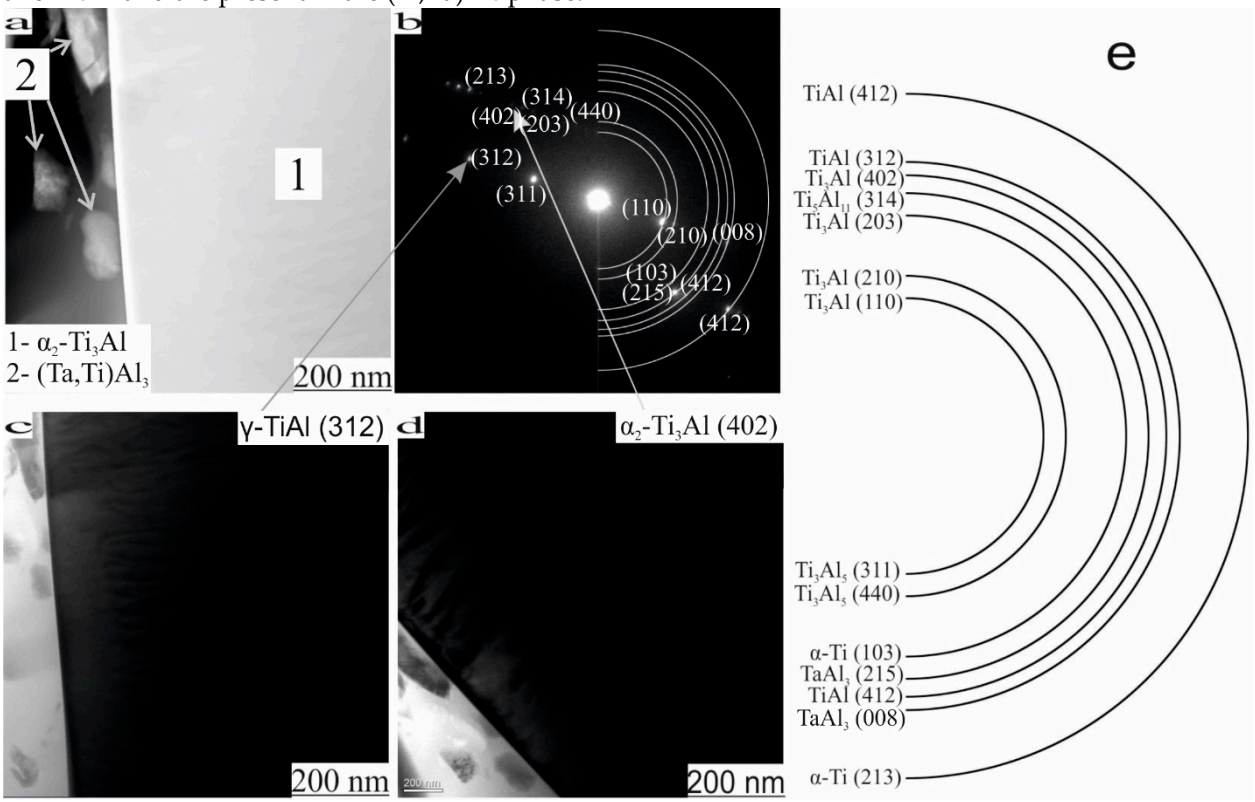


**Figure 9.** Electron microscope images of the TAT alloy: (**a)** bright-field image; (**b)** microdiffraction pattern; (**c)** dark-field image in reflex; (**d)** microdiffraction pattern identification.

Thus, the XPA and TEM studies have shown that the formed solid solution based on titanium and the alloys under study have particles of the new phase in their structure. It is also well known that after microalloying of the alloys with metals Y and Dy, the mass fraction of the TiAl phases increases significantly (>70%). A distribution of tantalum in the titanium–aluminum matrix is evidence of the possibility of the formation of the three component system $(Ti,Ta)Al_3$ [47–49]. Alloying metals, Y and Dy, form a compound with aluminum; they are applied as a dispersion phase and strengthen the alloy structure by the introduction of the second phase into the metal matrix in the form of a high-melting compound. If $YAl_2$ is located on the dislocations or on the grain boundaries, $DyAl_2$ is chaotically distributed in the grain volume.

## 4. Conclusion

The composite materials based on gamma-aluminides of titanium TiAl-REM were obtained by a new method—"hydride technology". The content of the major phases in the initial TA system, as well as TA-REM, containing microadditions Ta, Y and Dy, was determined by the Rietveld method with high reliability.

1. It was established that in the initial TA system and in the TA-REM system, containing microadditions, TiAl predominate in tetragonal and triclinic units. It was established that the used initial standard lattices, as well as the structures after the full-profile specification, were in the stable states.

2. The results of X-ray phase analysis are confirmed by the results of TEM. It is known that after microalloying alloys by Y and Dy metals, the mass fraction of TiAl phases increases significantly (>70%).

3. From the results of X-ray phase analysis and TEM studies, it follows that an insignificant amount of Ta dissolves in the crystals of TiAl and $Ti_3Al$ and are present in the (Ti,Ta)$Al_3$ phase. This fact indicates the possibility of the formation of a three component system (Ti, Ta)$Al_3$.

**Author Contributions:** Y.A. studied structural state and determined the energies of lattices of separate phases and fraction of quantitative phase, and wrote the paper; N.K conducted the microstructure research of samples and analyzed the data; I.K. conducted the X-ray phase analyses of samples; A.B. wrote the introduction and conducted the synthesis of samples; V.S. and R.E. analyzed data. All authors have read and agreed to the published version of the manuscript.

**Funding:** This work was carried out with the support of the Program of Competitive Recovery of TSU, NU 8.2.10.2018 L. and project No. 10.3031.2017/4.6.

**Acknowledgments:** The authors are grateful to Mark Kalashnikov for fruitful cooperation.

**Conflicts of Interest:** The authors declare no conflict of interest. The funding sponsors had no role in the design of the study; in the collection, analyses, or interpretation of data; in the writing of the manuscript, and in the decision to publish the results.

## References:

1. Clemens, H.; Chladil, H.; Wallgram, W.; Block, B.; Kremmer, S. In *Structural Aluminides for Elevated Temperature Applications;* Kim, Y.W., Morris, D., Yang, R., Leyens, C., Eds.; The Minerals, Metals and Materials Society (TMS): Warrendale, Michigan, USA, 2008; pp. 217–228.
2. Clemens, H.; Smarsly, W. Light-Weight Intermetallic Titanium Aluminides—Status of Research and Development. *Adv. Mater. Res.,* **2011**, *278*, 551–556, doi: 10.4028/www.scientific.net/AMR.278.551.
3. Appel, F.; Paul, J.D.; Oehring, M. *Science and Technology*, 1st ed.; Wiley-VCH: Weinheim, Germany, 2011.
4. Appel, F.; Clemens, H.; Fischer, F.D. Modeling concepts for intermetallic titanium aluminides. *Prog. Mater. Sci*., **2016**, *81*, 55–124, doi: 10.1016/j.pmatsci.2016.01.001.
5. Kurzina, I.A.; Kozlov, E.V.; Popova, N.A.; Kalinnikov, M.P.; Nikonenko, E.L.; Savkin, K.P.; Oks, E.M.; Sharkeev, Yu.P. Modifying the Structural Phase State of Fine Grained Titanium under Conditions of Ion Irradiation. *Bull. Rus. Acad. Sci., Physics*, **2012**, *76*, 1238–1245, doi: 10.3103/S1062873812110135.
6. Kurzina, I.A. Physical Base of the Metallic Gradient Surface Layers of Titanium Alloys Formed under Ion Implantation. *Adv. Mater. Res*., **2014**, *872*, 184–190, doi: 10.4028/www.scientific.net/AMR.872.184.
7. Zykova, A.P.; Kazantseva, L.A.; Kurzina, I.A.; Dammer, V.Kh.; Chumaevaskii, A.V. Influence of the Modifying Ability of Various Compositions on the Microstructure and Properties of the AK7ch Alloy. *Rus. J. Non-Ferrous Metals* **2015**, *56*, 593–598, doi: 10.3103/S1067821215060115.
8. Kurzina, I.; Nikonenko, A.; Popova, N.; Nikonenko, E.; Kalashnikov, M. Fine structure and phase composition of Fe-14Mn-1.2C steel: influe,nce of the modified mixture based on refractory metals. *Int. J. Miner*., **2017**, *24*, 523–529, doi: 10.1007/s12613-017-1433-2.
9. Kazantseva ,L.A.; Kurzina , I.A.; Kosova, N.I.; Pichugina, A.A.; Sachkov, V.I.; Vladimirov, A.A.; Sachkova, A.S. Synthesis of titanium hydrides and obtaining alloys based on them. *Bulletin Tomsk State University. Chemistry*, **2015**, *2*, 69–75.
10. Dolukhanyan, S.K.; Aleksanyan, A.G.; Ter-Galstyan, O.P.; Mailyan, D.G.; Shekhtman, V.Sh.; M. K. Sakharov, S. In *Carbon Nanomaterials in Clean Energy Hydrogen Systems*, Baranovski, B., Zaginaichenko, S., Schur, D., Skorokhod, V., Veziroglu, A, Eds; Springer: New York, NY, USA, 2008; pp. 733–741.
11. Hakobyan, H.; Aleksanyan, A.; Dolukhanyan, S.; Mnatsakanyan, N.; Shekhtman, V. In° *Solid state phenomena,* Bobet J. L, Ed.; Trans Tech Publications: Switzerland, 2011; p. 354.
12. Aleksanyan, A.G.; Dolukhanyan, S.K.; Shekhtman, V.Sh.; Khasanov, S.S.; Ter-Galstyan, O.P.; Martirosyan, M.V.; Formation of alloys in the TieNb system by hydride cycle method and synthesis of their hydrides in self-propagating high-temperature synthesis. *Int J Hydrogen Energy,* **2012**, *37,* 14234–14239, doi: 10.1016/j.ijhydene.2012.07.006.
13. Wallgram, W.; Schmolzer, T.; Cha, L.; Das, G.; Guther, V.; Clemens, H. Technology and mechanical properties of advanced γ-TiAl based alloys. *Int. J. Mater. Res.,* **2009**, *100*, 1021–1030, doi: 10.3139/146.110154.

14. Klein, T.; Rashkova, B.; Holec, D.; Clemens, H.; Mayer, S.; Advancement of Compositional and Microstructural Design of Intermetallic γ-TiAl Based Alloys Determined by Atom Probe Tomography. *Acta Mater*, **2016**, *110*, 236–245, doi: 10.1016/j.actamat.2016.03.050
15. Hadi, M.; Shafyei, A.; Meratian, M. A comparative study of microstructure and high temperature mechanical properties of a β-stabilized TiAl alloy modified by lanthanum and erbium. *Mater. Sci. Eng.*,**2015**, *624*, 1–8, doi: 10.1007/s11085-018-9842-9.
16. M. Bulanova, I. Fartushna, K. and A. Meleshevich, Samelyuk, Isothermal section at 850°C of the Ti–Dy–Al system in the Ti–TiAl–$DyAl_2$–Dyregion. *J. of Alloys and Comp.*, **2014**, *598*, 61–67, doi: 10.1016/j.jallcom.2014.01.250.
17. Hadi, M.; Shafyei, A.; Meratian, M.; Bayat, O.; Ebrahimzadeh, I. Oxidation Properties of a Beta-Stabilized TiAl Alloy. *Oxidation of Metals*, **2018**, *90*, 421–434, doi: 10.1007/s11085-018-9842-9.
18. Liu, Z.Z.G.; Chai ,L.H.; Chen ,Y.Y.; Kong, F.T.; Davies, H.A.; Figueroa, I.A. Microstructure evolution in rapidly solidified Y added TiAl ribbons. *Intermetallics*, **2011,** *19*, 160–164, doi: 10.1016/j.intermet.2010.08.023.
19. Wang, X.; Luo, R.; Liu, F.; Zhu, F.; Song, Sh. Characterization of Gd-rich precipitates in a fully lamellar TiAl alloy. *Scripta Materialia*, **2017**, *137*, 50–54, doi: 10.1016/j.scriptamat.2017.04.038.
20. Li, W.; Xia, K.; Kinetics of the $\alpha$ grain growth in a binary Ti–44Al alloy and a ternary Ti–44Al-0.15Gd alloy. *Mater. Sci. Eng.*, **2002**, A. 329-331, 430–434, doi: 10.1016/s0921-5093(01)01617-3 .
21. Xia, K.; Wu, X.; Song, D. Effects of Gd addition, lamellar spacing and loading direction on creep behavior of a fully lamellar Ti–44Al–1Mn–2.5Nb alloy. *Acta Mater.*, **2004**, *52*, 841–849, doi: 10.1016/j.actamat.2003.10.018.
22. Li, W.; Inkson, B.; Horita, Z.; Xia, K. Microstructure observations in rare earth element Gd-modified Ti-44 at%Al. *Intermetallics*, **2000**, *8*, 519–523, doi: 10.1016/s0966-9795(99)00156-9
23. Schwaighofer, E.; Clemens, H.; Lindemann, J.; Mayer**,** A,S. Hot-working behavior of an advanced intermetallic multi-phase γ-TiAl based alloy, *Mat. Sci. Eng*. **2014**, *77*, 297–310, doi: 10.1016/j.msea.2014.07.040.
24. Belgibaeva, A.A.; Erkasov, R.Sh.; Kurzina, I.A.; Karakchieva, N.I.; Sachkov, V.I.; Abzaev, Yu.A. *Obtainment of high-strength alloys of the Ti-Al system using "hydride technology"*, Proceedings of the conference New materials and technologies, Barnaul, Russia, 2018, pp. 62–66.
25. Kosova, N.; Sachkov, V.; Kurzina, I.; Pichugina, A.; Vladimirov, A.; Kazantseva, L.; Sachkova, A. The preparation of the Ti-Al alloys based on intermetallic phases. *IOP Conf. series: Mater. Sci. Eng.*, **2016**, *112*, 012039, doi: 10.1088/1757-899X/112/1/012039.
26. Abzaev, Yu.A.; Syzrantsev, V.V.; Bardakhanov, S.P. Simulation of the Structural State of Amorphous Phases in Nanoscale $SiO_2$ Synthesized via Different Methods. *Physics of the Solid State***, 2017**, *59*, 1850–854, doi: /10.1134/S1063783417090025.
27. Pecharsky, V.; Zavalij, P. *Fundamentals of powder diffraction and structural characterization of materials*, 2nd ed.; Springer: New York, NY, USA, 2005; p. 713.
28. Toby, B.H. R factors in Rietveld analysis: How good is good enough? *Powder Diffraction*, **2006**, *21*, 67–70, doi:10.1154/1.2179804
29. Young, R.A. *The Ritveld method*, Oxford University Press: Oxford, England, UK 1996.
30. Abdel-hamid, A.A. Influence of Ta, Zr, V and Mo on the growth-morphology of Ti-aluminide crystals. *Zeitschrift fur metallkunde***, 1991**, *82*, 383–386.
31. Crystallography Open Databasehttp://www.crystallography.net/cod/search.html;.2019 (accessed 13 March 2019).
32. Braun, J.; Ellner, M.; Predel, B.; Splat, *Z.* Splat-cooling investigations in the binary-system Ti-Al, *Metallkd.*, **1994**, *82*, 355–362.
33. Xie, Y.Q.; Peng, H.J.; Liu, X.B.; Peng, K.; Atomic states, potential energies, volumes, stability and brittleness of ordered FCC $Ti_3$Al-type alloys. *Physica*, **2005**, *B 362*, 1–17, doi: 10.1016/j.physb.2005.01.197.
34. Wang, H.Y.; Hu, Q.K.; Yang, W.P.; Li, X.Sh. Influence of metal element doping on the mechanical properties of TiAl alloy. *Acta physica sinica***, 2016**, *65*, 176101, doi: 10.7498/aps.65.077101.
35. Lyakhov, A.O.; Oganov, A.R.; Stokes, H.T.; Zhu, Q. New developments in evolutionary structure prediction algorithm USPEX. *Computer Physics Communications***, 2013**, *184*, 1172–1182, doi: 10.1016/j.cpc.2012.12.009.
36. Abzaev, Yu.A.; Starostenkov, M.D.; Klopotov, A.I.; First-principles calculations of the concentration dependence of elastic modules in monocrystals $Ni_3(Ge_{1-x},Al_x)$. *Fundamental problems of modern materials science*, **2014**, *11*, 56.
37. Segall, M.D.; Pickard, C.J.; Shah, R.; Payne, M.C. Population analysis in plane wave electronic structure calculations. *Mol. Phys*., **2010**, *89*, 571–577, doi: 10.1080/002689796173912.
38. Segall, M.D.; Shah, R.; Pickard, C.J.; Payne, M.C. Population analysis of plane-wave electronic structure calculations of bulk materials". *Phys. Rev*., **1996**, *B*, *54*, 16317–16320, doi: 10.1103/physrevb.54.16317.

39. Oganov, A.R.; Glass, C.W.; Lyakhov, A.O.; Zhu, Q.; Qian, G.R.; Stokes, H.T.; Bushlanov, P.Z.; Allahyari, S. Lepeshkin. Universal Structure Predictor: Evolutionary Xtallography. Manual. 9.7. Appendices.P.108. Electronic access: http://han.ess.sunysb.edu/.
40. Sereda, B.; Zherebtsov, A.; Belokon', Y. *The Modeling and Processes Research of Titan Aluminides Structurization Received by SHS Technology*, TMS.: Washington, USA, 2010; pp. 99–108.
41. Sereda, B.; Kruglyak, I.; Zherebtsov, A.; Belokon', Y.; *The Processes Research of Structurization of Titan Aluminides Received by SHS*, Materials Science & Technology: Pittsburg, USA, 2009; pp. 2069–2073.
42. Kurzina, I.A.; Kozlov, E.V.; Sharkeev, Yu.P.; Ryabchikov, A.I.; Stepanov, I.B.; Bozhko, I.A.; Kalashnikov, M.P.; Sivin, D.O.; Fortuna, S.V. Influence of ion implantation on nanoscale intermetallic-phase formation in Ti–Al, Ni–Al and Ni–Ti systems. *Surf. Coat. Technol.,* **2007,** *201*, 8463.
43. Imayev, V M.; Imayev, R.M.; Oleneva, T.I. Current status of γ-TiAl intermetallic alloys investigations and prospects for the technology developments. *Let. Mater.,* **2011**, *1*, 25.
44. Cordell, T. Titanium Aluminide Intermetallics. Advanced Materials and Processes Technology. *The AMPTIAC Newsletter*, **2000,** 4, 9.
45. Raghavan, V. Al-Ti-Y (Aluminum-Titanium-Yttrium). *Phase Equilibria and Diffusion*, **2005**, *26*, 191.
46. Zhou, H.; Liu, W.; Yuan, S.; Yan, J. The 500 °C Isothermal Section of the Al-Dy-Ti Ternary System. *Alloys and Compd.,* **2002**, *336*, 218–222.
47. Das K.; Das, S. A Review of the Ti-Al-Ta (Titanium-Aluminum-Tantalum) System. *Phase Equilibria and Diffusion*, **2005**, *26*, 323–24.
48. Sridharan, S.; Nowotny, H. Studies in the Ternary System Ti-Ta-Al and in the Quaternary System Ti-Ta-Al-C, *Z. Metallkd.*,**1983**, 74, 468–472.
49. McCullough, C.; Valencia, J.J.; Levi, C.G.; Mehrabian, R.; Maloney, M.; Hecht, R. Solidification Paths of Ti-Ta-Al Alloys. *Acta Metall.*, **1991**, 39, 2745–2758.